Capillary effects in guided crystallization of organic thin films

Alta Fang, Anna K. Hailey, Abigail Grosskopf, John E. Anthony, Yueh-Lin Loo, and Mikko Haataja

Citation: APL Materials **3**, 036107 (2015); doi: 10.1063/1.4915537
View online: http://dx.doi.org/10.1063/1.4915537
View Table of Contents: http://scitation.aip.org/content/aip/journal/aplmater/3/3?ver=pdfcov
Published by the AIP Publishing

Capillary effects in guided crystallization of organic thin films

Alta Fang,[1,a] Anna K. Hailey,[2,b] Abigail Grosskopf,[2,c] John E. Anthony,[3,d] Yueh-Lin Loo,[2,e] and Mikko Haataja[4,f]
[1]*Department of Mechanical and Aerospace Engineering, Princeton University, Princeton, New Jersey 08544, USA*
[2]*Department of Chemical and Biological Engineering, Princeton University, Princeton, New Jersey 08544, USA*
[3]*Department of Chemistry, University of Kentucky, Lexington, Kentucky 40506, USA*
[4]*Department of Mechanical and Aerospace Engineering, Princeton Institute for the Science and Technology of Materials (PRISM) and Program in Applied and Computational Mathematics (PACM), Princeton University, Princeton, New Jersey 08544, USA*

(Received 13 February 2015; accepted 9 March 2015; published online 19 March 2015)

Recently, it has been demonstrated that solvent-vapor-induced crystallization of triethylsilylethynyl anthradithiophene (TES ADT) thin films can be directed on millimeter length scales along arbitrary paths by controlling local crystal growth rates via pre-patterning the substrate. Here, we study the influence of capillary effects on crystallization along such channels. We first derive an analytical expression for the steady-state growth front velocity as a function of channel width and validate it with numerical simulations. Then, using data from TES ADT guided crystallization experiments, we extract a characteristic channel width, which provides the smallest feature size that can be obtained by this technique. [http://dx.doi.org/10.1063/1.4915537]

Guided crystallization of solution-processed organic semiconductor thin films via substrate patterning can enable the control of material properties with fine spatial resolution and be used to preferentially orient molecules along a given direction.[1,2] Potential applications of guided crystallization on pre-specified templates include the fabrication of patterned optical coatings or conductive paths with arbitrary shapes[1] as well as dense arrays of organic thin-film transistors.[2] In addition, the ability to control the alignment of organic semiconductor small molecules has been employed to study the effect of grain boundary orientation mismatch on electrical properties.[3]

Due to its limited intermolecular interactions, the small molecule organic semiconductor triethylsilylethynyl anthradithiophene (TES ADT) can be deposited in a thin film with an essentially disordered state and then be made to crystallize in the form of spherulites upon exposure to solvent vapor.[4–6] Spherulites are polycrystalline superstructures that are composed of crystalline grains of different orientations and grow outwards in a radially symmetric manner.[7] Recently, it has been shown that the crystallization rate of TES ADT can be controlled by varying the substrate surface energy, allowing growth to be guided along patterns on the millimeter length scale,[1] but application of this technique to smaller length scales has not previously been studied. More fundamentally, exploration of crystallization confined along narrow paths provides an opportunity to probe thermodynamic and interfacial properties[8,9] in such molecular semiconductor thin films. Often such

[a]alta@princeton.edu
[b]ahailey@princeton.edu
[c]akg@princeton.edu
[d]anthony@uky.edu
[e]lloo@princeton.edu
[f]mhaataja@princeton.edu

information is not known for materials other than metallic alloys.[10] An improved understanding of organic semiconductor molecular interactions and ordering behavior is also beneficial for better linking processing conditions to final structures.[11]

In this paper, we investigate how the rate of guided crystal growth in an initially disordered thin film along a pre-patterned two-dimensional (2D) channel of fixed width w is reduced with decreasing channel widths due to capillary effects. We first derive an analytical expression for the steady-state growth front velocity as a function of channel width and validate it against numerical simulations of a diffuse-interface model. We show that, below a characteristic channel width, capillary effects strongly affect crystallization. In particular, in the case of perfect confinement of the crystal growth front within the channel, this characteristic channel width determines the smallest feature size that can be achieved by guided crystallization. Finally, analytical results are employed to determine the characteristic channel width (given by the ratio of interfacial energy to bulk thermodynamic driving force) for solvent-vapor-annealed TES ADT from channel crystallization experiments.

Our starting point is the observation that the growth velocity normal to the interface ($\hat{\mathbf{n}}$) of a crystallization front, V_n, and its shape are affected by both interfacial and bulk thermodynamic driving forces[8,12–14] via $V_n = M(\hat{\mathbf{n}})[-\gamma(\hat{\mathbf{n}})\kappa + E]$. Here, $M(\hat{\mathbf{n}})$ is a kinetic coefficient related to the molecular mobility (in general anisotropic) of an interface, $\gamma(\hat{\mathbf{n}})$ denotes the so-called interface stiffness[15] given by $\Gamma + \Gamma''$, where $\Gamma(\hat{\mathbf{n}})$ denotes interfacial tension (in general anisotropic) and $\Gamma''(\hat{\mathbf{n}})$ its second derivative with respect to interface inclination, κ is the curvature of the interface, and E is the bulk driving force. For effectively isotropic systems (such as spherulites[16,17]), the interface equation of motion simplifies to

$$V_n = M[-\Gamma\kappa + E]. \tag{1}$$

We note that bulk measurements of V_n only report the product ME and not M or E independently.

Now, for guided crystallization in the configuration shown in Fig. 1(a), Eq. (1) in steady-state reduces to $\frac{w_c}{2}\frac{d^2y/dx^2}{[1+(dy/dx)^2]^{3/2}} + 1 = \frac{V/V_{max}}{\sqrt{1+(dy/dx)^2}}$, where $y(x)$ denotes the interface shape. Furthermore, $V_{max} \equiv ME$ and $w_c \equiv \frac{2\Gamma}{E}$, while M, E, and Γ refer to values within the channel. In principle, solving this non-linear differential equation subject to boundary conditions $dy/dx|_{x=\pm w/2} = \mp\sqrt{\left(\frac{V}{rV_{max}}\right)^2 - 1}$ and $dy/dx|_{x=0} = 0$ yields both the steady-state growth front velocity V and growth front shape $y(x)$. Here, we have defined $V_{out} = rV_{max}$ to be the growth velocity outside of the channel, with $0 \le r < 1$ denoting the leakage rate. While the exact solution for $y(x)$ at non-zero

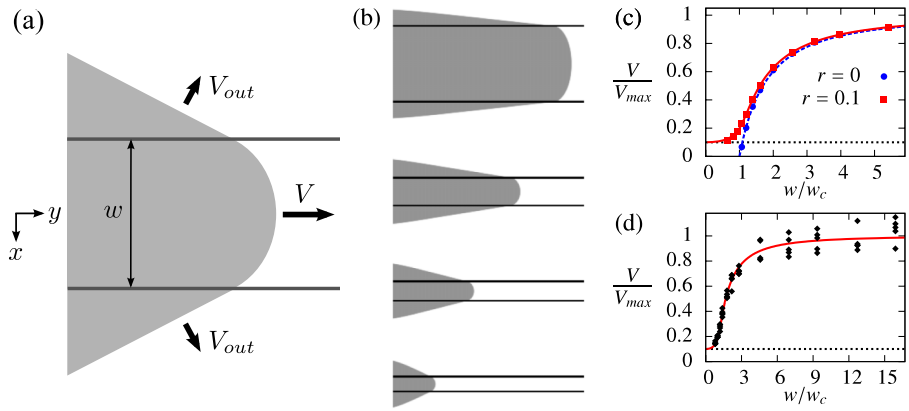

FIG. 1. (a) Schematic of guided crystallization. Inside (outside) a channel of width w, the growth front propagates at velocity V (V_{out}) and adopts a curved (planar) shape. (b) Simultaneously captured steady-state growth morphologies from numerical simulations of isotropic single crystal systems with channel widths w/w_c = 5.4, 2.0, 1.4, and 1.1 for leakage rate $r = 0.1$. (c) Normalized growth velocity as a function of w/w_c. The blue dashed and red solid curves are fits to Eq. (2) for $r = 0$ and $r = 0.1$, respectively, while the black dotted line indicates $V/V_{max} = 0.1$, where V_{max} denotes the asymptotic growth velocity achieved for $w/w_c \to \infty$. (d) Normalized growth velocity from simulations of polycrystalline systems with five different initial conditions, for $r = 0.1$. The red solid curve again is a fit to Eq. (2).

V has eluded us, the dependence of V on w can be obtained in terms of an implicit formula without any approximations,[18]

$$\frac{w}{w_c} = \frac{V_{max}}{VA}\left[-A\tan^{-1}(s) + \tan^{-1}\left(\frac{s}{A}\right) + \tan^{-1}\left(\frac{rs}{A}\right)\right], \tag{2}$$

where $A \equiv \sqrt{1-\left(\frac{V}{V_{max}}\right)^2}$ and $s \equiv \sqrt{\left(\frac{V}{rV_{max}}\right)^2 - 1}$.

Equation (2) constitutes the central analytical result of this paper. It can be readily deduced that (a) at the characteristic width $w = w_c = \frac{2\Gamma}{E}$, growth becomes completely arrested due to capillary effects for $r = 0$, in agreement with exploratory simulations reported in Ref. 19. (b) For $w \ll w_c$, $V \to rV_{max}$. In this limit, growth is dominated by bulk crystallization outside the channel. (c) For $w \gg w_c$, $V \to V_{max} = ME$, as expected for bulk crystallization within the channel. (d) Perhaps most importantly, experimentally measuring $V = V(w)$ and fitting to Eq. (2) allows the characteristic width $w_c = 2\Gamma/E$ to be determined. (e) Finally, a more convenient-yet-accurate approximation can be derived by assuming that the growth front takes on an elliptical shape, yielding[18]

$$\frac{w}{w_c} \approx (1-r)^{-1/3}\frac{\sqrt{1-\left(\frac{rV_{max}}{V}\right)^2}}{\left(1-\frac{V}{V_{max}}\right)^{2/3}}. \tag{3}$$

We note that in the limit where $r = 0$, indicating perfect confinement, Eq. (3) implies a simple scaling relation $V \approx V_{max}\left[1-(w/w_c)^{-3/2}\right]$.

To validate Eq. (2), we turn to numerical simulations of a simple diffuse-interface model,[20] wherein a continuously varying order parameter $\phi(\mathbf{r},t)$ is introduced to track the locations of different phases as they evolve over time. The free energy of the system is described by a Ginzburg-Landau free energy functional that accounts for both interfacial and bulk free energies via $F = \int d\mathbf{r}\left(\frac{\epsilon^2}{2}|\nabla\phi|^2 + f(\phi)\right)$, where $f(\phi) = \frac{1}{4}\phi^4 + \frac{m-3/2}{3}\phi^3 - \frac{m-1/2}{2}\phi^2$. As usual, the spatio-temporal evolution of ϕ is governed by the Allen-Cahn equation $\frac{\partial\phi}{\partial t} = -\tilde{M}(\mathbf{r})\frac{\delta F}{\delta\phi} = \tilde{M}(\mathbf{r})\left(\epsilon^2\nabla^2\phi - \frac{\partial f}{\partial\phi}\right)$. In the limit of a sharp interface between the phases,[13] this evolution equation leads to phase boundary motion described by Eq. (1) with spatially modulated M and constant Γ.

We numerically solve the diffuse-interface equations using finite differences and explicit time stepping on a uniform grid with non-dimensionalized parameters $N_y = 1500, \Delta x = 0.01, N_t = 420\,000, \Delta t = 2\times10^{-6}, \tilde{M} = 2\times10^5, \epsilon^2 = 4\times10^{-5}$, and $m = 0.01$. In our simulations, we model the effect of a surface-energy-defined channel by setting the molecular mobility $\tilde{M}$ outside of the channel to be a fraction $r = M_{out}/M_{in}$ of the mobility inside of the channel; the effects reported herein are the same if the bulk driving force were spatially modulated instead of the mobility. Note that in this paper, mobility always refers to molecular motion rather than to electrical mobility. We model the film as 2D and initialize the film in the metastable amorphous phase ($\phi = 0$) everywhere except for a circular seed of the crystalline phase ($\phi = 1$) at the center of the channel.

First, we perform simulations with $r = 0.1$ such that the emerging crystalline phase is only partially confined within the channel. Several simultaneously captured configurations of the crystalline phase for different channel widths are shown in Fig. 1(b). In these configurations, the crystalline phase is shown in gray, while the white regions correspond to the amorphous phase. It can be seen that the growth front is flatter and thus moves faster for wider channels. Figure 1(c) in turn shows that the velocity of the growth front is quantitatively described by Eq. (2) and approaches the outside growth rate rV_{max} as $w \to 0$. Finally, in the case of perfect confinement corresponding to $r = 0$, the growth front velocity vanishes below the characteristic channel width w_c [cf. Fig. 1(c)]. This observation implies that w_c sets the smallest feature size that can be obtained via guided crystallization.

In order to observe these capillary effects experimentally, we tracked the crystallization of thin films of TES ADT on patterned substrates during solvent vapor annealing, following the experimental procedure outlined in the supplementary material.[18] Since crystal growth occurs several times faster on SiO_2 than on pentafluorobenzenethiol (PFBT)-treated Au, crystallization can be guided along channels defined on the substrate by regions of SiO_2 surrounded by regions of

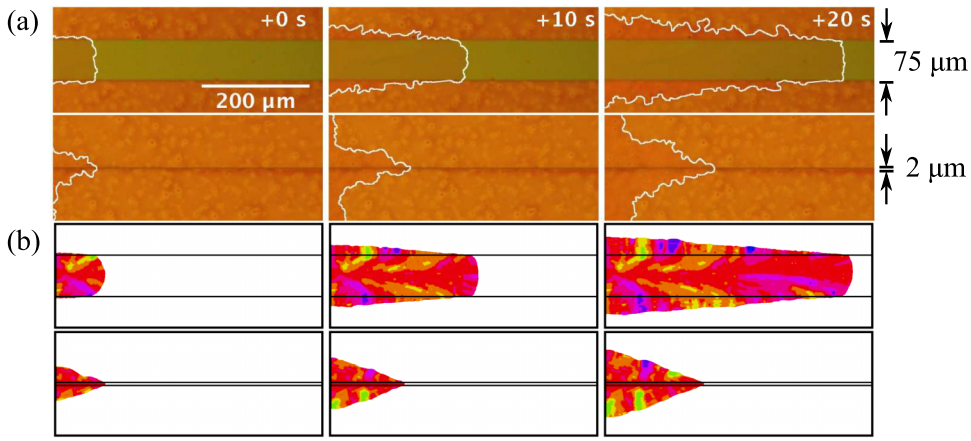

FIG. 2. (a) Optical micrographs of TES ADT crystallization show that crystal growth occurs preferentially on bare SiO_2 (green) compared to PFBT-treated Au substrate (orange). The crystal-amorphous interface is traced in white. Crystallization proceeds faster in the 75 ± 0.33 μm-wide channel (top) than in the 2 ± 0.33 μm-wide channel (bottom). (b) Numerical simulations of polycrystalline growth exhibit similar behavior. Colors represent differently oriented crystalline grains, while the yet-to-crystallize regions are shown in white.

PFBT-treated Au. Figure 2(a) shows optical micrographs of TES ADT as crystallization takes place along channels with widths of 75 ± 0.33 and 2 ± 0.33 μm during solvent vapor annealing, demonstrating qualitatively that growth velocity decreases for narrower widths. Since crystallization also proceeds on PFBT-treated Au regions, confinement of crystal growth to the surface-energy-defined channel is not perfect and leads to shapes that resemble those of the numerical simulations shown in Fig. 1(b). Furthermore, in solvent-vapor-annealed TES ADT, the crystalline phase is actually polycrystalline with many differently oriented grains separated by grain boundaries,[1] so the shape of the growth front is not completely smooth. To explore the effects of polycrystallinity and interfacial roughness on channel growth kinetics, we performed additional numerical simulations of the diffuse-interface model described in Ref. 21, which has previously been applied to study growth of spherulites in organic thin films. We use non-dimensionalized parameters $N_t = 26\,000$, $M_{max} = 5 \times 10^4$, $\Delta t = 2.4 \times 10^{-5}$, $N_y = 1024$, $\Delta x = \Delta y = 0.01$, $\epsilon^2 = 2 \times 10^{-5}$, $\alpha = 0.12, \delta_\theta = 0.2$, $\Delta = 20$, $k_B T = 1.6 \times 10^{-6}$, $l^2 = 3.2 \times 10^{-4}$, and $r = 0.1$. Figure 2(b) shows simulated morphologies demonstrating qualitatively that capillary slowing is still observed for polycrystalline growth. In addition, Fig. 1(d) shows that across five independent simulations of polycrystalline growth, growth front velocity is quantitatively described by Eq. (2) within the scatter of the data.

Finally, we quantitatively compare the experimentally measured crystal growth velocity behavior against our theoretical predictions. To this end, Fig. 3 shows that for channel widths greater than approximately 20 μm, capillary effects are negligible and the growth velocity is effectively constant, but growth rate falls rapidly for smaller w. The solid blue curve in Fig. 3 shows a fit of the experimental data to Eq. (2) with rV_{max} fixed to equal the average measured growth rate on PFBT-treated Au. The fit yielded a characteristic channel width of $w_c = 2\Gamma/E = 3.7 \pm 1.2$ μm, where the error bar represents a range of reasonable fits based on visual quality of the fit.

In order to estimate the physical value for E, we can use Turnbull's empirical formula[22] to estimate the solid-liquid interfacial energy of a material from its heat of fusion, giving $\Gamma \approx 7$ mJ/m^2 for TES ADT. Since this represents only a rough estimate,[9,23] we can more conservatively hypothesize (based on the solid-liquid surface energies of several other organic compounds[23]) that the TES ADT crystal-amorphous interfacial energy ranges from $\Gamma \approx 5$ to 50 mJ/m^2. Using this range of values for Γ along with the value for w_c extracted from the experimental data, we find that the free energy difference between the as-spun disordered phase and the more stable spherulitic phase ranges from $E \approx 1.3$ to 13 J/mol for TES ADT, corresponding to an equivalent undercooling of TES ADT of 0.05–0.5 °C. Interfacial mobility M in turn is estimated to range from $M \approx 1.3 \times 10^{-6}$ to 1.3×10^{-5} m mol/J s for the same system.

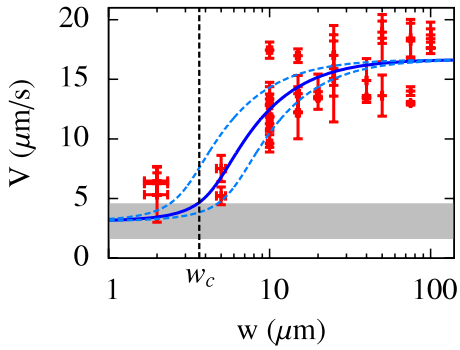

FIG. 3. Experimentally measured growth front velocity V as a function of channel width w. As w approaches zero, V approaches the growth rate on PFBT-treated Au, indicated by the thick gray line whose thickness indicates one standard deviation about the average. Horizontal error bars represent ± 0.33 μm channel width resolution and vertical error bars indicate one standard deviation of velocity measurements. The solid blue curve is a fit to Eq. (2) and the light-blue dashed curves show Eq. (2) with $w_c = 2\Gamma/E = 3.7 \pm 1.2$ μm.

In summary, we have derived an analytical expression for interfacial velocity when a phase transformation is guided along a straight channel defined by differential growth rates. We verified our theoretical predictions with simulations of a diffuse-interface model and employed analytical expressions to extract the characteristic channel width (that is, the ratio of the surface energy of the crystal-amorphous interface to the bulk thermodynamic driving force for crystallization) below which capillary effects strongly influence crystallization in TES ADT. More broadly, we expect that our approach will enable the quantification of important material parameters for crystallization in a wide range of organic thin-film systems.

A.F. and A.K.H. acknowledge the National Science Foundation for Graduate Research Fellowships under Grant No. DGE 1148900. A.G. acknowledges the Princeton Environmental Institute through the Grand Challenges Program for summer funding. Y.-L.L. and J.E.A. acknowledge NSF funding through the SOLAR Initiative (Nos. DMR-1035217 and DMR-1035257) and Y.-L.L. acknowledges MRSEC funding through the Princeton Center for Complex Materials (No. DMR-0819860). The authors would also like to thank Dr. Srevatsan Muralidharan for helpful discussions and his contributions during the initial stages of this work.

[1] S. S. Lee, S. B. Tang, D.-M. Smilgies, A. R. Woll, M. A. Loth, J. M. Mativetsky, J. E. Anthony, and Y.-L. Loo, Adv. Mater. **24**, 2692 (2012).
[2] G. Giri, S. Park, M. Vosgueritchian, M. M. Shulaker, and Z. Bao, Adv. Mater. **26**, 487 (2014).
[3] S. S. Lee, J. M. Mativetsky, M. A. Loth, J. E. Anthony, and Y.-L. Loo, ACS Nano **6**, 9879 (2012).
[4] M. M. Payne, S. A. Odom, S. R. Parkin, and J. E. Anthony, Org. Lett. **6**, 3325 (2004).
[5] K. C. Dickey, T. J. Smith, K. J. Stevenson, S. Subramanian, J. E. Anthony, and Y.-L. Loo, Chem. Mater. **19**, 5210 (2007).
[6] K. Dickey, J. Anthony, and Y.-L. Loo, Adv. Mater. **18**, 1721 (2006).
[7] H. D. Keith and J. F. J. Padden, J. Appl. Phys. **34**, 2409 (1963).
[8] A. Skapski, R. Billups, and A. Rooney, J. Chem. Phys. **26**, 1350 (1957).
[9] D. Jones, J. Mater. Sci. **9**, 1 (1974).
[10] L. Granasy, L. Ratkai, A. Szallas, B. Korbuly, G. I. Toth, L. Kornyei, and T. Pusztai, Metall. Mater. Trans. A **45**, 1694 (2014).
[11] A. M. Hiszpanski and Y.-L. Loo, Energy Environ. Sci. **7**, 592 (2014).
[12] K. R. Elder, M. Grant, N. Provatas, and J. M. Kosterlitz, Phys. Rev. E **64**, 021604 (2001).
[13] N. Provatas and K. Elder, *Phase-Field Methods in Materials Science and Engineering* (Wiley-VCH, 2010), pp. 39–42.
[14] G. Gottstein and L. Shvindlerman, *Grain Boundary Migration in Metals: Thermodynamics, Kinetics, Applications*, Materials Science & Technology, 2nd ed. (Taylor & Francis, 2009).
[15] D. Du, H. Zhang, and D. J. Srolovitz, Acta Mater. **55**, 467 (2007).
[16] M. Jabbour, C.-S. Man, and R. Paroni, J. Chem. Phys. **139**, 144704 (2013).
[17] C.-S. Man, M. Jabbour, R. Paroni, Y.-L. Loo, A. K. Hailey, S. S. Lee, J. E. Anthony, and M. A. Loth, "Spherulitic crystallization in binary thin films under solvent-vapor annealing. ii. Small-molecule semiconductor and additive" (unpublished).
[18] See supplementary material at http://dx.doi.org/10.1063/1.4915537 for additional information on the experimental procedure and analytical derivations.
[19] S. Muralidharan, "Continuum studies of microstructure formation in metallic and organic thin films," Ph.D. thesis (Department of Mechanical and Aerospace Engineering, Princeton University, 2012).
[20] R. Kobayashi, Phys. D **63**, 410 (1993).
[21] A. Fang and M. Haataja, Phys. Rev. E **89**, 022407 (2014).
[22] D. Turnbull, J. Appl. Phys. **21**, 1022 (1950).
[23] H. Lu, Z. Wen, and Q. Jiang, J. Phys. Org. Chem. **20**, 236 (2007).